https://doi.org/10.5194/egusphere-2025-1503
Preprint. Discussion started: 21 May 2025

Developing A Custom-Built Metal Cloud Chamber: Analysis of Aerosol Coagulation at Low Humidities.

Nevil A. Franco, Kyle J. Gorkowski, Katherine B. Benedict

Earth and Environmental Science Division, Los Alamos National Laboratory, P.O. Box 1663
Los Alamos, NM, US 87545-1663

Corresponding Authors: Kyle Gorkowski (gorkowski@lanl.gov), Katherine Benedict (kbenedict@lanl.gov)

Abstract

We are developing an intermediate size (906 L) cloud chamber, and this paper reports on the design and initial characterization of dry aerosol experiments. Specifically, we are determining wall-loss and coagulation correction factors using the observed size distribution measurements for surrogates of common aerosol classes: sodium chloride, sucrose, and soot. Results show that, on average, sodium chloride, sucrose, and soot wall-loss rates converge to similar values on relatively short time scales (<1 hour). The fitted coagulation correction factor, W_C^{-1}, for soot particles (1.23 ± 0.312), indicates they adhere to each other more than sodium chloride

https://doi.org/10.5194/egusphere-2025-1503
Preprint. Discussion started: 21 May 2025

(0.969 ± 0.524) and sucrose (1.16 ± 1.38). This study lays the foundation for future experiments at elevated humidity and supersaturation conditions to characterize the influence of particle shape on coagulation and cloud parameters.

1 Introduction

Aerosol-cloud interactions remain one of the largest sources of uncertainty in the Earth's radiation budget. By directly scattering, absorbing solar radiation and indirectly influencing cloud formation, aerosols affect longwave and shortwave radiation in the Earth's atmosphere[1]. Despite sustained research efforts, these impacts still pose significant challenges to our understanding of the aerosol cooling effect, estimated at -0.86 ± 0.56 W/m^2, and the effective anthropogenic radiative forcing of Earth's climate (estimated at -1.25 ± 0.85 W/m^2)[1]. The complexity of aerosol sources, properties, and processing continues to hinder precise quantification of these forcing estimates.

A critical source of aerosols is wildfire smoke, which can influence radiative budgets up to a year depending on the transport and evolution of plumes[2–4]. Under extreme burning conditions, wildfires can generate pyrocumulonimbus clouds, lofting large concentrations of aerosol into the upper troposphere and lower stratosphere[2,5,6]. These smoke particles can exert prolonged effects on climate through chemical and physical processes such as condensation and coagulation[7–9]. The fractal nature of soot particles further complicates our understanding of their indirect effects on cloud formation and radiative properties[10–12]. For instance, during the Amazon biomass burning season, Koren et. al.[13] reported a dramatic reduction in cumulus cloud

https://doi.org/10.5194/egusphere-2025-1503
Preprint. Discussion started: 21 May 2025

cover—from 38% under cleaner conditions to 0% during heavy smoke. However, Kaufman & Koren et. al.[14] observed an increased cloud cover in regions with higher column aerosol concentrations. These discrepancies underscore the complexity of aerosol-cloud interactions, which depend on various factors such as aerosol composition, hygroscopicity, size distribution, supersaturation, and the prevailing atmospheric stability[15]. As wildfires increase in frequency and intensity due to climate change[16], refining our knowledge of how these aerosols evolve and ultimately affect cloud development is crucial for improving climate models and future predictions.

Beyond large-scale aerosol effects, aging aerosols undergo microphysical transformations that can drastically alter their role in cloud processes. Condensation of organics and the mixing of sulfate with black carbon (BC) have both been shown to influence cloud dynamics[17]. Recent work indicates that larger BC agglomerates may form preferentially at cloud tops, while the heaviest-coated BC particles are most likely to be scavenged by cloud droplets[18,19]. Modeling these highly dynamic processes remains challenging, as it requires accurately representing particle growth, mixing states, and cloud interactions[20–24].

Cloud chambers are valuable research tools for investigating microphysical mechanisms under well-controlled conditions[25–28]. Existing cloud chambers are their own institutional facility in the case of CLOUD at CERN[29], AIDA Chamber EUROCHAMP[30], and PI-chamber at MTU[26]. All chambers however, come with artifacts—most notably, the loss of particles to chamber walls through gravity, diffusion, convection, and electrostatic forces[31–34]. Previous studies have

https://doi.org/10.5194/egusphere-2025-1503
Preprint. Discussion started: 21 May 2025

highlighted the importance of accounting for both size-dependent and time-dependent wall losses[35,36].

In this paper, we introduce the development of a Los Alamos National Laboratory (LANL) cloud chamber, which is specifically designed to investigate coagulation processes under simulated conditions. We present initial data from experiments where aerosols were injected in a dry environment to quantify losses to chamber walls, dilution, and coagulation effects. Different types of aerosols were examined to validate known aerosol behaviors and characterize coagulation. We further demonstrate the use of a python based aerosol package, Particula[37], to model coagulation and wall-loss rates. Through these studies, we aim to refine experimental design and advance understanding of how aerosols—particularly soot—undergo physical transformations that shape their role in cloud formation and climate forcing.

2 Chamber Development and Methods

2.1 Setup of chamber and experiments

The LANL chamber is in the first phase of development with control of both temperature and humidity to be added in future work. The 906 L chamber is made of 6 stainless steel walls which are inert and reduce the effects of electrostatic charge. The rectangular body and dimensions are shown in Figure 1. The chamber's joints are sealed with a fast cure marine adhesive caulk (Sika, Sikaflex 291) and the outside junctions where the walls intersected were

https://doi.org/10.5194/egusphere-2025-1503
Preprint. Discussion started: 21 May 2025

sealed using ZIP System™ Strech Tape (Huber Engineered Woods). Portholes were made for the top and bottom plates where wires and probes be placed for measurements in the chamber and for aerosols to flow in and out of the chamber. Unused portholes are sealed with Swagelok caps and those used for probes and wires are sealed with a rubber gasket or a Teflon ferrule. A leak test was performed by pressurizing the chamber by feeding clean air in and sealing every outlet then seal any leak detected.

Copper tubing lines (3/8") are used to supply aerosols to the chamber and deliver outflow sampling to instrumentation. Zero-air generators (T701 Teledyne Inc., USA) provide clean dry air to push aerosol to the chamber and additional dilution air using Teflon tubing (1/4"). Push flow enters at the bottom of the chamber, creating an upwards direction of flow. Aerosols are sampled from an outlet at the top of the chamber. A dilution flow is connected to the outlet line (88.9 mm from the outlet) to control aerosol concentrations and prevent overwhelming the sampling instruments. A minimum sampling flow rate of 1.5 L/min was needed to supply the instruments and we used a 1:5 ratio of push to dilution for the experiments presented here. This infers a residence timescale within the chamber of 604 minutes (10 hours) and half-life of 418 minutes (6.9 hours). The flow rates are controlled with mass flow controllers (MFC; Alicat). Prior to each experiment the chamber was flushed by pushing clean air with a flow of ~10 L/min for at least 3 hours to reach background (~0-10 cm^{-3}).

https://doi.org/10.5194/egusphere-2025-1503
Preprint. Discussion started: 21 May 2025

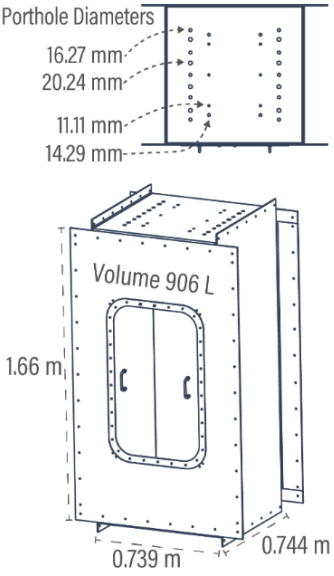

Figure 1. Schematic of LANL's 906 L chamber. The chamber has external dimensions of 1.66 m in height, 0.739 m in width, and 0.744 m in depth. The design includes 56 portholes with diameters ranging from 11.11 mm to 20.24 mm, shown across the top and mirrored on the bottom.

2.2 Aerosol Generation and Instrumentation

Two aqueous solutions and controlled combustion of dried biomaterial were used as the sources of aerosols. Sodium chloride (NaCl; Sigma-Aldrich) was chosen because it is a well-understood compound in aerosol studies. Sucrose (Sigma-Aldrich) was used to act as a secondary organic aerosol surrogate, and it is also a well-studied aerosol. Each were dissolved in deionized water (Milli-Q, 18.2 MΩ) in separate solutions and were put on an Atomizer Aerosol Generator (3079, TSI Inc., USA). The particles coming out of the atomizer passed through a silica

https://doi.org/10.5194/egusphere-2025-1503
Preprint. Discussion started: 21 May 2025

gel diffusion drier at a generation flow rate of ~2.4 L/min. The duration of aerosol injection varied based on the desired number concentration. To generate soot, 0.1 – 0.5 g samples of dried biomaterial *Poa pratensis* (Kentucky bluegrass) were weighed out, placed on a quartz boat and into a quartz-tube furnace (Carbolite Gero, TS1-1200, Verder Scientific, UK) that was set to 1000°C for a flaming combustion condition. Soot particles were pushed to the chamber by zero-air at 4 L/min for 5 minutes, an estimated time for complete combustion of the sample.

Aerosol size and number distributions downstream of the cloud chamber were measured with a scanning mobility particle sizer (SMPS) that consists of a Differential Mobility Analyzer (3081 DMA, TSI Inc., USA) and a Condensation Particle Counter (3752, TSI Inc., USA). Measurement settings were set to continuously scan for 3 minutes/scan; 160 seconds recording with 20 seconds of purging, measuring sizes 15.7 – 764.5 nm. Our experimental matrix consisted of 5 repeats of NaCl, 4 repeats of sucrose and 6 soot experiments with varying biomaterial mass, they are outlined in Supplement Information Table 1. In all experiments the first 6 hours of data were used to analyze results.

https://doi.org/10.5194/egusphere-2025-1503
Preprint. Discussion started: 21 May 2025

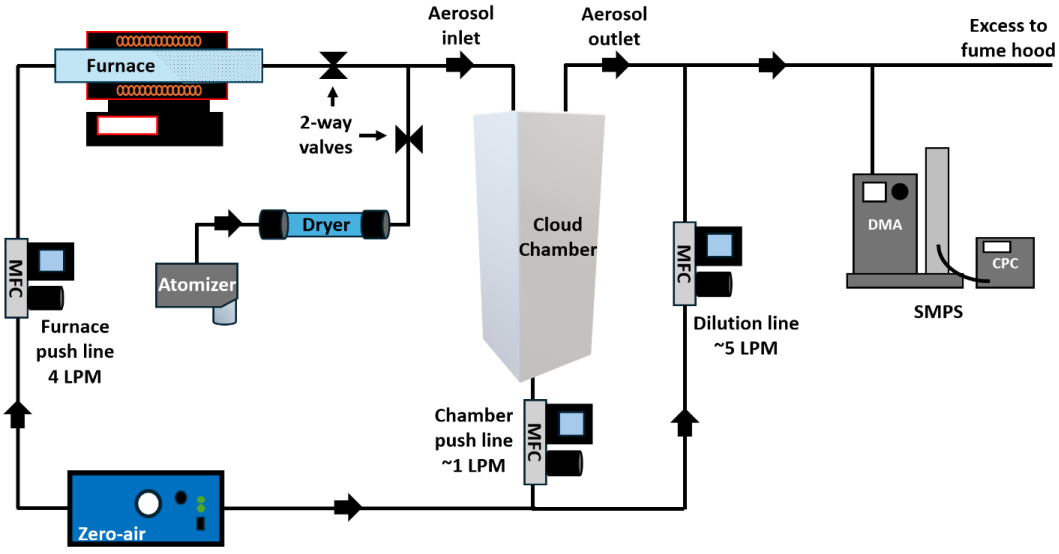

Figure 2. Schematic of experimental setup showing how aerosols are injected and sampled from the chamber.

3 Theory on Chamber Processes

The processing of data from the LANL chamber experiments involved two key steps to analyze the underlying aerosol processes of coagulation, wall loss, and dilution (chamber push line). First, we determined the observed size-dependent particle rates: $dN(D_p)/dt$. The measured size distributions were fitted to a two-mode lognormal distribution. The lognormal distribution parameters were optimized using the Python library SciPy's optimization routines, with the mean squared error as the cost function. We used multiple minimization methods and selected the best fit for each timestep based on the highest Pearson R-squared value. The

https://doi.org/10.5194/egusphere-2025-1503
Preprint. Discussion started: 21 May 2025

methods included Nelder-Mead (Simplex algorithm), Powell's method (Powell's conjugate direction method), L-BFGS-B (Limited-memory Broyden-Fletcher-Goldfarb-Shanno with Box constraints), TNC (Truncated Newton Conjugate-Gradient method), SLSQP (Sequential Least Squares Programming), and trust-constr (Trust Region Constrained method).

Second, we fitted these observed rates to theoretical rates calculated from Particula[37], a python-based aerosol microphysics package. The first step was to generate a new time series at a higher size resolution (log-spaced 250 bins), extrapolating to lower (20 nm) and upper (4 µm) diameter limits. The size-dependent particle rate was then computed as the linear slope of 21 point moving window (10 before and 10 after). This final rate was subsequently used to fit the underlying aerosol processes in Equation 1 where $N(D_p)$ represents the number concentration of particles of diameter, D_p, K_{12} is the coagulation kernel, W_C^{-1} is the coagulation correction factor, N_1 and N_2 are the concentrations of particles in the bins for K_{12}, k_{flow} is the dilution rate, and β is the wall-loss rate.

$$\frac{dN(D_p)}{dt} = W_C^{-1} K_{12} N_1 N_2 - k_{flow} N(Dp) - \beta N(Dp) \qquad \text{Equation 1}$$

The coagulation term is governed by a Brownian Coagulation kernel, K_{12}, that captures the collision frequency between bin number concentrations (N_1 and N_2). This kernel is described in Seinfeld and Pandis[38] (Section 13; Fuchs form with alpha efficiency form of 13.56), and calculated with Particula. Since K_{12} does not account for other interactions (e.g. Coulomb interactions) that may lead to coagulation, W_C^{-1}, the coagulation correction factor, was

https://doi.org/10.5194/egusphere-2025-1503
Preprint. Discussion started: 21 May 2025

determined. In our analysis, W_C^{-1} is a free fit parameter to allow for un-modeled behaviors to be represented. The dilution rate, $k_{flow} = Q/V$, characterizes how the clean air flow rate (Q) is used to push sample flow out of the chamber volume (V). Finally, the wall-loss term, $\beta \mathrm{N(Dp)}$, accounts for the size-dependent removal of particles to the chamber walls.

$$\beta = \frac{1}{LWH}\left(\frac{4H\,(L+W)\,\sqrt{k_e D}}{\pi} + v_p\,LW \times coth\left(\frac{\pi v_p}{4\sqrt{k_e D}}\right)\right) \qquad \text{Equation 2}$$

Equation 2 shows the wall-loss rate (β) varies with particle size, derived from a rectangular-chamber formulation adapted from Crump and Seinfeld[35] and Crump[36]. It incorporates both diffusion-driven transport and gravitational settling. In this formulation, L, W, and H denote the chamber's length, width, and height, respectively; k_e is the eddy wall diffusivity (a free fit parameter); D is the particle diffusion coefficient; and v_p is the particle gravitational settling velocity.

4 Results and Discussion

4.1 Example Analysis

We show, in Figure 3, the L-BFGS-B optimization routine that was used on Equation 1 for experimental data from the smoke aerosol generated by combusting Kentucky bluegrass. Figure 3a shows the lognormal-fitted size distribution for the entire experiment, where particle growth is evident as the mode diameter shifts to larger sizes over the six-hour period. Figure 3b breaks

https://doi.org/10.5194/egusphere-2025-1503
Preprint. Discussion started: 21 May 2025

down the observed rates after 1.5 hours into three calculated, time-varying, size-dependent components: coagulation, dilution, and wall-loss. At that time, coagulation dominates, reducing particles around 100 nm (~0.16 cm^{-3} s^{-1}) and forming larger particles around 200 nm. From these fits we are specifically interested in the kernel correction factor to better understand the importance of agglomeration of freshly emitted BC fractal-like particles and how it changes in time.

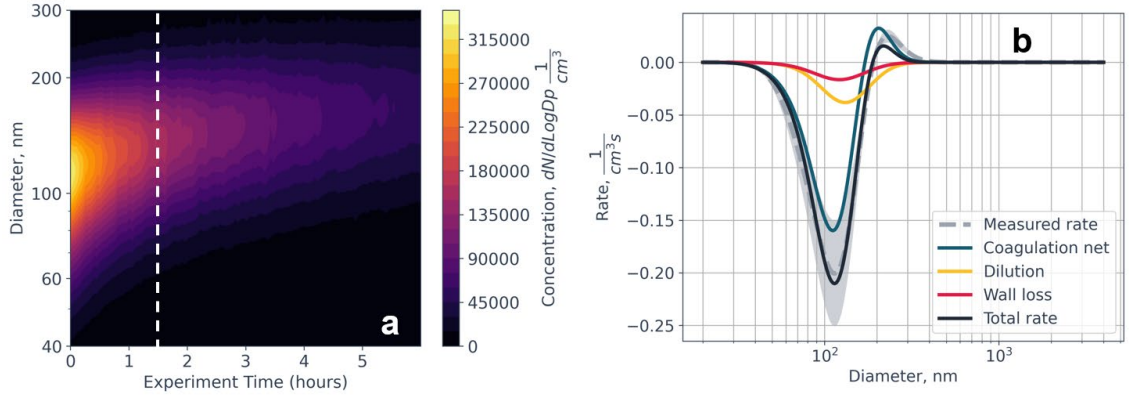

Figure 3. **a)** Time series of the lognormal-fitted size distribution and concentration for a soot experiment. The dashed line marks a time slice at approximately 1.5 hours. **b)** At this time slice, particle loss rates are calculated, revealing both loss and gain of particles due to coagulation. (The time series of rates for individual aerosol species are provided in the Supplement.) In this panel, the dashed gray line represents the measured rate with uncertainty (shaded gray), while the blue, yellow, and pink lines correspond to the coagulation process, dilution, and wall loss, respectively.

https://doi.org/10.5194/egusphere-2025-1503
Preprint. Discussion started: 21 May 2025

4.2 Wall-loss Comparison

In Figure 4a we show the average wall-loss rates for our three different aerosol types based on 4–8 experiments each. Only results with valid optimizations and an R-squared above 0.85 were included. In the sucrose experiments, this filter led to data gaps during the later time periods (2–6 hours) for inclusion in the analysis. To better compare with soot, we conducted additional NaCl experiments to have a more complete timeseries for one of the comparisons. The wall-loss rates during the first hour (< 1 hour) follow a similar trend apart from NaCl starting at a low wall-loss rate then rising close to a rate of 2 s^{-1}. These initial wall-loss rates are consistent with the general observation in chamber studies that early mixing processes and injection conditions can dominate particle loss. Typical ranges reported in smog-chamber experiments span from < 1 s^{-1} to tens of s^{-1} depending on injection flow and the use of a fan[39], particle species[40,41], and chamber geometry[40]. Over longer times (>1 hours), all three aerosol types converge toward similar wall-loss rates, in agreement with the literature indicating that chamber turbulence and gravitational settling diminish over time as mixing subsides.

Figure 4b shows the statistical distribution of the wall-loss rates for each aerosol type during the first hour and the subsequent five hours. NaCl and sucrose do not exhibit a large variance in diffusivity for the first hour compared to soot which is 1.12 ± 1.55 s^{-1}. NaCl, sucrose, and soot show mean wall-loss rates of 0.562 ± 0.975 s^{-1}, 0.233 ± 0.286 s^{-1}, and 0.201 ± 0.267 s^{-1}, respectively. This convergence to relatively similar values is consistent with past observations in

https://doi.org/10.5194/egusphere-2025-1503
Preprint. Discussion started: 21 May 2025

207 smog-chamber experiments, where turbulent mixing dissipates, and the system approaches a
208 quasi-steady loss rate such as the CMU Teflon chamber[33,34], the CESAM chamber[40], and the AIR
209 chamber[39]. However, NaCl and soot sucrose experiments display greater variability than soot,
210 likely due to residual chamber turbulence and differences in particle surface charge stemming
211 from their distinct generation methods (aerosolization vs. combustion).

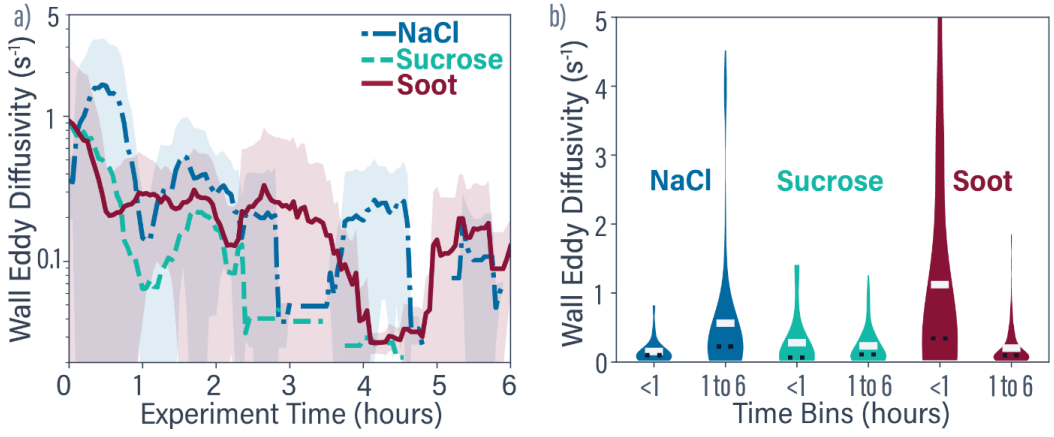

212

213 Figure 4. a) Average time series of the calculated wall eddy diffusivity for NaCl (blue), sucrose
214 (green), and soot (red). Only fits with valid optimizations and r-squared greater than 0.85 are
215 included. b) Violin plots showing the mean (**..**), median (white bar) and overall distribution
216 range of wall eddy diffusivity values for each aerosol type in two-time bins (<1 hour and 1–6
217 hours). The width of each colored region represents the relative density of data points at that
218 value.

219

https://doi.org/10.5194/egusphere-2025-1503
Preprint. Discussion started: 21 May 2025

4.3 Coagulation Corrections

To investigate the influence of interparticle forces on aerosol coagulation, we fitted a coagulation correction factor that would account for van der Waals forces, shape, and/or Coulomb interactions in the coagulation rate. When $W_C^{-1} = 1$, collisions are effectively "elastic," with no net enhancement or inhibition. In contrast, $W_C^{-1} > 1$ indicates that coagulation is enhanced (e.g. due to attractive forces, favorable particle morphology, or turbulence), whereas $W_C^{-1} < 1$ implies reduced coagulation (e.g. electrostatic repulsion or other inhibiting effects).

In figure 5a., the soot experiments show an initial period where $W_C^{-1} > 1$, which may be explained by the fractal nature of soot aggregates that can promote sticking or chain formation upon collision. By the third hour in all experiments, accounting for the variation the average coagulation corrections extend above and below 1. During this later phase, particle concentrations ($< 3 \times 10^3$ cm^{-3}) no longer sustain significant coagulation losses, consistent with prior studies showing that coagulation becomes negligible under low concentration conditions[34,42,43].

Figure 5b shows the distribution of coagulation corrections for these time periods. All three aerosols show a mean W_C^{-1} value around 1 (0.969 ± 0.524 for NaCl, 1.16 ± 1.38 for sucrose, and 1.23 ± 0.312 for soot), suggesting a slight repulsion or negligible net sticking among particles. However, the standard deviations do encompass $W_C^{-1} = 1$. Soot exhibits a slightly higher coagulation corrections initially followed by reduced values (0.941 ± 0.307) in later periods. These observations align with the notion that both particle morphology (e.g.,

https://doi.org/10.5194/egusphere-2025-1503
Preprint. Discussion started: 21 May 2025

240 fractal soot structures) and injection-induced turbulence can transiently enhance coagulation,
241 but the effect diminishes as particles coagulate.

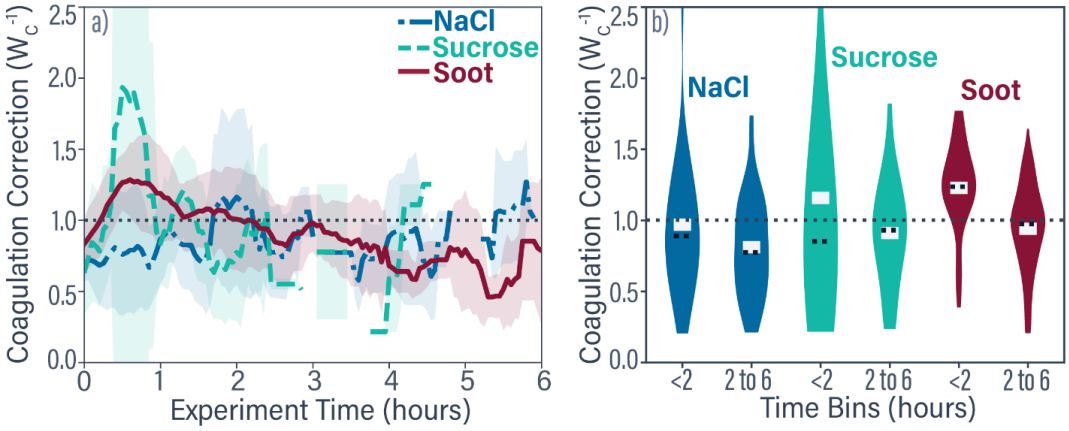

242

243 Figure 5. a) Average time series of the calculated coagulation correction for NaCl (blue), sucrose
244 (green), and soot (red). Only fits with valid optimizations and r-squared greater than 0.85 are
245 included. b) Violin plots showing the mean (**..**), median (white bar) and range of the calculated
246 coagulation correction for each aerosol type averaged across replicate experiments for the
247 indicated time bins (similar to Figure 4b).

248

249 **5 Discussion**

250 Our initial experiments in this new cloud chamber focused on dry conditions and a set of
251 aerosols to quantify how particles evolve in the absence of humidity (<10% relative humidity).
252 Despite the relatively simple setup—no temperature or humidity control—two key insights will

https://doi.org/10.5194/egusphere-2025-1503
Preprint. Discussion started: 21 May 2025

be used in future humidified experiments. First, the wall-loss rates converged to similar values across all aerosol types after the first hour, indicating that early differences largely arose from injection flow conditions and subsequent turbulence. Over time, these chamber conditions stabilized, reinforcing the well-documented notion that particle wall losses approach a quasi-steady state as mixing subsides.

A second important finding is that coagulation within the chamber is most pronounced during the initial phase of each experiment. Though this is more uncertain due to larger relative errors. Soot showed signs of coagulation enhancement, potentially attributable to its fractal structure. Once total number concentrations fell below a few thousand particles per cubic centimeter, coagulation slowed considerably, consistent with the literature. Collectively, these observations highlight the dynamic interplay between wall loss, particle morphology, and injection protocols in shaping the early stages of aerosol evolution in chamber studies.

Our results also shed light on the influence of particle composition and shape. While aerosols like NaCl and sucrose exhibited expected behavior—initial collision enhancements near unity—soot displayed additional complexity. Early-time coagulation factors for soot were moderately elevated, suggesting that fractal aggregates can promote sticking or increased collisional radius. Over longer times, the coagulation rates for all three aerosols converged to near unity or below, indicating negligible net enhancement under steady-state conditions. These observations set the stage for more detailed investigations of fractal-like particles under high humidity environments (>90% relative humidity).

https://doi.org/10.5194/egusphere-2025-1503
Preprint. Discussion started: 21 May 2025

Although these initial experiments focused on low humidities, the chamber design allows for temperature and humidity control to be integrated in future work. Extending to more complex atmospherically relevant aerosol mixtures—such as soot mixed with organic vapors or inorganic salts—will further elucidate aerosol aging pathways and cloud interactions. Additionally, the use of more advanced aerosol instrumentation will improve the characterization of particle morphologies and mixing states that evolve during cloud processing.

6 Conclusion

The custom-built 906 L stainless-steel chamber provided reproducible measurements of particle size distributions under dry conditions, confirming its suitability for controlled aerosol research. Although initial turbulence drove high wall-loss rates, these converged to stable values across NaCl, sucrose, and soot—underscoring that injection protocols and mixing strongly influence early aerosol behavior. The chamber's intermediate size and flexible design for future temperature and humidity controls make it a useful platform to investigate aerosol-cloud interactions more comprehensively. Integrating additional measurements of particle shape, chemical composition, and mixing state will further clarify the complexities of aerosol aging and cloud formation. Building on these dry experiments, upcoming work at higher humidity will reveal how aerosol coagulation and phase changes affect cloud processes such as droplet activation and scavenging. By disentangling coagulation, dilution, and wall-loss mechanisms, this chamber ultimately enables rigorous study of aerosol transformations—particularly for

https://doi.org/10.5194/egusphere-2025-1503
Preprint. Discussion started: 21 May 2025

fractal soot—in cloud-relevant environments, helping advance both scientific understanding and climate prediction.

Author contributions. NAF performed the experiments, contributed to the analysis of the results, and wrote the manuscript. KJG was responsible for the design of the chamber and the study, development of the data analysis methods, and contributed to the writing of the manuscript. KBB contributed to the design of the study, analysis of the results, and contributed to the writing of the manuscript.

Competing interests. The authors declare no competing interests.

Code/Data availability. The python data analysis code is available from corresponding authors.

Acknowledgments. The authors would like to thank Hannah Brink, Ryan Farley, James E. Lee, and Matt Nelson for their feedback on the manuscript. Release Number LA-UR-25-22994.

Financial support. Research presented in this article was supported by the Laboratory Directed Research and Development program of Los Alamos National Laboratory under project number

https://doi.org/10.5194/egusphere-2025-1503
Preprint. Discussion started: 21 May 2025

20230248ER. This work was supported by the U.S. Department of Energy through the Los Alamos National Laboratory. Los Alamos National Laboratory is operated by Triad National Security, LLC, for the National Nuclear Security Administration of U.S. Department of Energy (Contract No. 89233218CNA000001).

References

1. Intergovernmental Panel On Climate Change (Ipcc). *Climate Change 2021 – The Physical Science Basis: Working Group I Contribution to the Sixth Assessment Report of the Intergovernmental Panel on Climate Change*. (Cambridge University Press, 2023). doi:10.1017/9781009157896.

2. Yu, P. *et al.* Black carbon lofts wildfire smoke high into the stratosphere to form a persistent plume. *Science* **365**, 587–590 (2019).

3. D'Angelo, G., Guimond, S., Reisner, J., Peterson, D. A. & Dubey, M. Contrasting Stratospheric Smoke Mass and Lifetime From 2017 Canadian and 2019/2020 Australian Megafires: Global Simulations and Satellite Observations. *JGR Atmospheres* **127**, e2021JD036249 (2022).

4. Guimond, S. R., Reisner, J. & Dubey, M. The Dynamics of Megafire Smoke Plumes in Climate Models: Why a Converged Solution Matters for Physical Interpretations. *J Adv Model Earth Syst* **15**, e2022MS003432 (2023).

https://doi.org/10.5194/egusphere-2025-1503
Preprint. Discussion started: 21 May 2025

5. Rodriguez, B., Lareau, N. P., Kingsmill, D. E. & Clements, C. B. Extreme Pyroconvective Updrafts During a Megafire. *Geophysical Research Letters* **47**, e2020GL089001 (2020).

6. Leach, R. N. & Gibson, C. V. Assessing the Potential for Pyroconvection and Wildfire Blow Ups. *J. Operational Meteor.* 47–61 (2021) doi:10.15191/nwajom.2021.0904.

7. Fromm, M., Servranckx, R., Stocks, B. J. & Peterson, D. A. Understanding the critical elements of the pyrocumulonimbus storm sparked by high-intensity wildland fire. *Commun Earth Environ* **3**, 243 (2022).

8. Reisner, J. M. *et al.* Informed Multi-Scale Approach Applied to the British Columbia Fires of Late Summer 2017. *JGR Atmospheres* **128**, e2022JD037238 (2023).

9. Gorkowski, K. *et al.* Insights into Pyrocumulus aerosol composition: black carbon content and organic vapor condensation. *Environ. Sci.: Atmos.* **4**, 80–87 (2024).

10. Cotton, W. R. & Anthes, R. A. *Storm and Cloud Dynamics*. (Academic Press, San Diego, 2010).

11. Das, S., Colarco, P. R., Oman, L. D., Taha, G. & Torres, O. The long-term transport and radiative impacts of the 2017 British Columbia pyrocumulonimbus smoke aerosols in the stratosphere. *Atmos. Chem. Phys.* **21**, 12069–12090 (2021).

12. June, N. A. *et al.* Aerosol size distribution changes in FIREX-AQ biomass burning plumes: the impact of plume concentration on coagulation and OA condensation/evaporation. *Atmos. Chem. Phys.* **22**, 12803–12825 (2022).

https://doi.org/10.5194/egusphere-2025-1503
Preprint. Discussion started: 21 May 2025

13. Koren, I., Kaufman, Y. J., Remer, L. A. & Martins, J. V. Measurement of the Effect of Amazon Smoke on Inhibition of Cloud Formation. *Science* **303**, 1342–1345 (2004).

14. Kaufman, Y. J. & Koren, I. Smoke and Pollution Aerosol Effect on Cloud Cover. *Science* **313**, 655–658 (2006).

15. Feingold, G., Remer, L. A., Ramaprasad, J. & Kaufman, Y. J. Analysis of smoke impact on clouds in Brazilian biomass burning regions: An extension of Twomey's approach. *J. Geophys. Res.* **106**, 22907–22922 (2001).

16. Cunningham, C. X., Williamson, G. J. & Bowman, D. M. J. S. Increasing frequency and intensity of the most extreme wildfires on Earth. *Nat Ecol Evol* **8**, 1420–1425 (2024).

17. Ching, J., West, M. & Riemer, N. Quantifying Impacts of Aerosol Mixing State on Nucleation-Scavenging of Black Carbon Aerosol Particles. *Atmosphere* **9**, 17 (2018).

18. Taylor, J. W. *et al.* Size-dependent wet removal of black carbon in Canadian biomass burning plumes. *Atmos. Chem. Phys.* **14**, 13755–13771 (2014).

19. Zanatta, M. *et al.* Airborne investigation of black carbon interaction with low-level, persistent, mixed-phase clouds in the Arctic summer. *Atmos. Chem. Phys.* **23**, 7955–7973 (2023).

20. Riemer, N., West, M., Zaveri, R. A. & Easter, R. C. Simulating the evolution of soot mixing state with a particle-resolved aerosol model. *J. Geophys. Res.* **114**, 2008JD011073 (2009).

https://doi.org/10.5194/egusphere-2025-1503
Preprint. Discussion started: 21 May 2025

21. Zaveri, R. A., Barnard, J. C., Easter, R. C., Riemer, N. & West, M. Particle-resolved simulation of aerosol size, composition, mixing state, and the associated optical and cloud condensation nuclei activation properties in an evolving urban plume. *J. Geophys. Res.* **115**, 2009JD013616 (2010).

22. Ching, J., Riemer, N. & West, M. Black carbon mixing state impacts on cloud microphysical properties: Effects of aerosol plume and environmental conditions. *JGR Atmospheres* **121**, 5990–6013 (2016).

23. Yao, Y., Dawson, M. L., Dabdub, D. & Riemer, N. Evaluating the Impacts of Cloud Processing on Resuspended Aerosol Particles After Cloud Evaporation Using a Particle-Resolved Model. *JGR Atmospheres* **126**, e2021JD034992 (2021).

24. Yang, F., Hoffmann, F., Shaw, R. A., Ovchinnikov, M. & Vogelmann, A. M. An Intercomparison of Large-Eddy Simulations of a Convection Cloud Chamber Using Haze-Capable Bin and Lagrangian Cloud Microphysics Schemes. *J Adv Model Earth Syst* **15**, e2022MS003270 (2023).

25. Khlystou, A., Kos, G. P. A. & Ten Brink, H. M. A High-Flow Turbulent Cloud Chamber. *Aerosol Science and Technology* **24**, 59–68 (1996).

26. Chang, K. *et al.* A Laboratory Facility to Study Gas–Aerosol–Cloud Interactions in a Turbulent Environment: The Π Chamber. *Bulletin of the American Meteorological Society* **97**, 2343–2358 (2016).

https://doi.org/10.5194/egusphere-2025-1503
Preprint. Discussion started: 21 May 2025

27. Niedermeier, D. *et al.* Characterization and first results from LACIS-T: a moist-air wind tunnel to study aerosol–cloud–turbulence interactions. *Atmos. Meas. Tech.* **13**, 2015–2033 (2020).

28. Shao, Y. *et al.* Characterisation of the Manchester Aerosol Chamber facility. *Atmos. Meas. Tech.* **15**, 539–559 (2022).

29. The Cloud Collaboration. A study of the link between cosmic rays and clouds with a cloud chamber at the CERN PS. Preprint at https://doi.org/10.48550/ARXIV.PHYSICS/0104048 (2001).

30. Wagner, R. *et al.* Chamber Simulations of Cloud Chemistry: The AIDA Chamber. in *Environmental Simulation Chambers: Application to Atmospheric Chemical Processes* (eds. Barnes, I. & Rudzinski, K. J.) vol. 62 67–82 (Kluwer Academic Publishers, Dordrecht, 2006).

31. Corner, J. & Pendlebury, E. D. The Coagulation and Deposition of a Stirred Aerosol. *Proc. Phys. Soc. B* **64**, 645–654 (1951).

32. Fotou, G. P. & Pratsinis, S. E. A Correlation for Particle Wall Losses by Diffusion in Dilution Chambers. *Aerosol Science and Technology* **18**, 213–218 (1993).

33. Wang, N., Jorga, S. D., Pierce, J. R., Donahue, N. M. & Pandis, S. N. Particle wall-loss correction methods in smog chamber experiments. *Atmos. Meas. Tech.* **11**, 6577–6588 (2018).

https://doi.org/10.5194/egusphere-2025-1503
Preprint. Discussion started: 21 May 2025

34. Mahfouz, N. G. A. & Donahue, N. M. Primary ion diffusion charging and particle wall loss in smog chamber experiments. *Aerosol Science and Technology* **54**, 1058–1069 (2020).

35. Crump, J. G. & Seinfeld, J. H. Turbulent deposition and gravitational sedimentation of an aerosol in a vessel of arbitrary shape. *Journal of Aerosol Science* **12**, 405–415 (1981).

36. Crump, J. G., Flagan, R. C. & Seinfeld, J. H. Particle Wall Loss Rates in Vessels. *Aerosol Science and Technology* **2**, 303–309 (1982).

37. Particula [computer software]. uncscode/particula: v0.1.3. Zenodo https://doi.org/10.5281/ZENODO.6634653 (2025).

38. Seinfeld, J. H. & Pandis, S. N. *Atmospheric Chemistry and Physics: From Air Pollution to Climate Change*. (John Wiley & Sons, Incorporated, Newark, 2016).

39. Zong, T. *et al.* A new smog chamber system for atmospheric multiphase chemistry study: design and characterization. *Atmos. Meas. Tech.* **16**, 3679–3692 (2023).

40. Wang, J. *et al.* Design of a new multi-phase experimental simulation chamber for atmospheric photosmog, aerosol and cloud chemistry research. *Atmos. Meas. Tech.* **4**, 2465–2494 (2011).

41. Li, K. *et al.* Smog chamber study on aging of combustion soot in isoprene/SO2/NOx system: Changes of mass, size, effective density, morphology and mixing state. *Atmospheric Research* **184**, 139–148 (2017).

https://doi.org/10.5194/egusphere-2025-1503
Preprint. Discussion started: 21 May 2025

421 42. Hussein, T. *et al.* Deposition rates on smooth surfaces and coagulation of aerosol
422 particles inside a test chamber. *Atmospheric Environment* **43**, 905–914 (2009).

423 43. Yu, H. *et al.* Experimental and Numerical Study on the Gravitational Deposition and
424 Coagulation of Aerosols. *Front. Energy Res.* **10**, 840503 (2022).

425